J|A|C|S ARTICLES

Published on Web 02/10/2009

Simulation of Self-Assembly of Cationic Lipids and DNA into Structured Complexes

Oded Farago[†] and Niels Grønbech-Jensen*[,‡]

Department of Biomedical Engineering, Ben Gurion University, Be'er Sheva 84105, Israel, and Department of Applied Science, University of California, Davis, California 95616

Received September 25, 2008; E-mail: ngjensen@ucdavis.edu

Abstract: We present a comprehensive set of simulations that elucidates several features of experimentally observed self-assembled structures in solutions of DNA and mixtures of neutral and cationic lipids. Our simulations are based on the Noguchi−Takasu implicit-solvent coarse-grained model of lipids as rigid trimer molecules [Noguchi, H.; Takasu, M. *Phys. Rev. E* **2001**, *64*, 041913.]. This model is extended in our work so that a certain fraction, ϕ_c, of the lipids carries +1e charge and DNA molecules are introduced as uniformly charged rods. The simplified coarse-grained modeling approach provides a feasible way to study the long time-scale dynamics associated with the evolution of mesoscopically large complexes from initially disordered systems. Our simulations show that, depending on the rigidity parameter κ_s which governs the stiffness of the membranes, both lamellar and inverted hexagonal complexes are formed at intermediate charged lipid densities. Disordered structures are formed both when large amounts of neutral lipids (small ϕ_c) are introduced which leads to the "erosion" of the spatial order, as well as for large charge densities that result in membrane rupture. A novel phase, where DNA rods and cylindrical micelles form a two-dimensional square lattice analogous to the three-dimensional cubic NaCl-type structure, is observed in the large ϕ_c regime for very soft membrane material ($\kappa_s = 0$).

Introduction

Somatic gene therapy holds great promise for future medical applications, for example, as new treatment for various inherited diseases and cancers.[1,2] Viral vectors have been the most widely used systems for this purpose,[3,4] but synthetic nonviral vectors are emerging as an attractive alternative because of their inherent advantages.[5−7] These advantages include ease and variable preparation, unlimited length of the transported DNA, and lack of specific immune response due to the absence of viral peptide and proteins.[7−9] Complexes consisting of cationic lipids (CLs) and DNA comprise one of the most promising classes of nonviral vectors. They are already used widely for *in vitro* transfection of mammalian cells in research applications, and have even reached the stage of empirical clinical trials.[10] Currently, their efficiency of gene transfer is considerably lower than that of viral vectors,[11,12] and substantial improvement of their efficiency is required before CL−DNA complexes will be viable for therapeutic purposes.

The improvement of CL−DNA vectors requires a better understanding of their mechanism of transfection and the chemical and physical parameters of CL−DNA complexes influencing it. According to a recently proposed model of cell entry, transfection is viewed as a two-stage process involving adsorption and entry (via endocytosis) of the CL−DNA complex into the cell, followed by the release of the DNA to the cytoplasm and delivery to the nucleus.[12−14] The transfection efficiency (TE) is largely dependent on the rate of the second step, i.e., the ability of the negatively charged DNA to dissociate from the cationic lipids. Some studies have suggested that the morphologies and structure of the CL−DNA complex may be critical factors affecting TE dramatically.[12,15] The two predominant phases of CL−DNA complexes are (a) the multilamellar phase where DNA monolayers are intercalated between lipid bilayers (L_α^C),[16] and (b) the inverted hexagonal phase with DNA encapsulated within monolayers tubes and arranged on a two-

[†] Ben Gurion University.
[‡] University of California, Davis.

(1) Felgner, P. L.; Rhodes, G. *Nature* **1991**, *349*, 351–352.
(2) Smyth-Templeton, N., Lasic, D. D., Eds. *Gene Therapy. Therapeutic Mechanisms and Strategies*; Marcel Dekker Inc.: New York, 2000.
(3) Smith, A. E. *Annu. Rev. Microbiol.* **1995**, *49*, 807–838.
(4) Kay, M. A.; Glorioso, J. C.; Naldini, L. *Nat. Med.* **2001**, *7*, 33–40.
(5) Felgner, P. L., Heller, M. J., Lehn, P., Behr, J.-P., Szoka, F. C., Eds. *Artificial Self-Assembling Systems for Gene Delivery*; American Chemical Society: Washington DC, 1996.
(6) Miller, A. D. *Angew. Chem., Int. Ed.* **1998**, *37*, 1768–1785.
(7) Huang, L., Hung, M. C., Wagner, E., Eds. *Non-Viral Vectors for Gene Therapy*; Academic Press: San Diego, 1999.
(8) Mahato, R. I., Kim, S. W., Eds. *Pharmaceutical Perspectives of Nucleic Acid-Based Therapeutics*; Taylor and Francis: London, New York, 2002.
(9) Kamiya, H.; Tsuchiya, H.; Yamazaki, J.; Harashima, H. *Adv. Drug Delivery Rev.* **2001**, *52*, 153–164.
(10) Edelstein, M. L.; Abedi, M. R.; Wixon, J. *J. Gene Med.* **2007**, *9*, 833–842.
(11) Willard, H. F. *Science* **2000**, *290*, 1308–1309.
(12) Ewert, K.; Slack, N. L.; Ahmad, A.; Evans, H. M.; Lin, A. J.; Samuel, C. E.; Safinya, C. R. *Curr. Med. Chem.* **2004**, *11*, 133–149.
(13) Huebner, S.; Battersby, B. J.; Grimm, R.; Cevc, G. *Biophys. J.* **1999**, *76*, 3158–3166.
(14) Kennedy, M. T.; Pozharski, E. V.; Rakhmanova, V. A.; MacDonald, R. C. *Biophys. J.* **2000**, *78*, 1620–1633.
(15) Smisterova, J.; Wagenaar, A.; Stuart, M. C. A.; Polushkin, E.; ten Brinke, G.; Hulst, R.; Engbert, J. B. F. N.; Hoekstra, D. *J. Biol. Chem.* **2001**, *276*, 47615–47622.
(16) Rädler, J. O.; Koltover, I.; Salditt, T.; Safinya, C. R. *Science* **1997**, *275*, 810–814.

dimensional (2D) hexagonal lattice (H_{II}^C).[17] The inverted hexagonal phase exhibits high TE that does not depend on σ_M, the cationic surface charge density.[12,15] In contrast, the TE of the lamellar phase appears to be strongly dependent on σ_M, and is considerably lower than the high TE of the H_{II}^C at both low and high charge densities.[18−20] The superior transfection of the inverted hexagonal phase has been attributed to the less stable nature of its bounding membrane (having positive rather than the preferred negative curvature) which greatly reduces the activation energy for fusion of H_{II}^C complexes with the endosomal membrane.

The viewpoint that a critical factor in lipid-mediated transfection is the structural evolution of lipoplexes upon interacting and fusing with the cellular membrane has received considerable support recently.[21] Two cationic phospholipids with asymmetric hydrocarbon chains, oleoyldecanoyl−ethylphosphatidylcholine (C18:1/C10-EPC) and stearoyldecanoyl−ethylphosphatidylcholine (C18:0/C10-EPC), were found to exhibit ∼50-fold difference in their DNA transfection efficiency in human umbilical artery endothelial cells. The former is the more efficient transfection agent, presumably because it undergoes a lamellar−nonlamellar phase transition when mixed with anionic membrane lipid formulations, while the latter maintains its (stable) lamellar structure. Improved TE has been also found for CL−DNA complexes containing multivalent CLs (MVLs).[19] MVLs with a dendritic headgroup that carries up to 16 positive charges have recently been synthesized. The large headgroup size induces the formation of a new ordered phase, termed H_I^C, where the hexagonally arranged tubular lipid micelles are surrounded by DNA rods forming a three-dimensional (3D) continuous substructure with honeycomb symmetry.[22] It has been speculated that the high TE of the H_I^C complex (in four different cell lines, including mouse embryonic fibroblasts which are empirically known to be hard to transfect) may be due to the existence of a continuous DNA substructure facilitating the release of the DNA cargo. In another recent work, the TEs of two CL−DNA complexes consisting of isomeric CLs with the same headgroup, the same hydrophobic tails, and the same ester linker functionality have been compared in four cultured mammalian cells.[23] The only difference between the molecular structures of the two CLs was the orientation of the ester group which was found to have a dramatic influence on the TEs. The remarkably higher TE of one of the CLs (CL-1) compared to that of the other (CL-2) was attributed to the lower rigidity and higher fluidity of the CL-1 liposomes, which enable them to fuse more efficiently, than the CL-2 liposomes, with both the plasma and endosomal membranes.

Our current perception of transfection pathways and the parameters affecting TE is based on a large body of experimental work using different characterization techniques such as X-ray diffraction and electron microscopy, as well as a variety of gene expression essays. Validation of these concepts and further insight can be gained from computer simulations providing a molecular level picture of the structure and dynamics of CL−DNA complexes. For reasons of computational complexity, atomistic level simulations of CL−DNA complexes[24] are not possible if one attempts to study mesoscopically large systems. Such systems can be addressed only through coarse grained (CG) models in which both the lipids and DNA molecules are represented in a simplified manner. This modeling approach is consistent with the well-established viewpoint that much of the meso-scale behavior of CL−DNA complexes is dominated by nonspecific electrostatic, elastic, and entropic forces that are insensitive to the fine molecular details.[25−27] Recently developed *implicit solvent* coarse-grained (ISCG) bilayer membrane models, where water is modeled implicitly by the use of intermolecular potentials effectively mimicking the hydrophobic effect, represent a promising approach for large-scale simulations of biomolecular assemblies.[28] An ISCG membrane model has been recently extended for simulations of CL−DNA lamellar complexes providing clear evidence for the formation of membrane pores as a result of increasing the concentration of CLs.[29,30] This and other computational findings suggest that the elevated electrostatic stress may be responsible for the complex loss of mechanical stability, which may explain the observed enhanced TE of lamellar complexes at high charge densities. The existence of an inverse correlation between the stability and transfection activity was further supported by ISCG simulations of lamellar complexes of multivalent CLs and DNA.[20]

In this work, we present molecular simulations of the self-assembly of CL−DNA complexes. Our studies, which are carried out on systems much larger than those simulated before, provide new insight into the structural phase diagram of the system. Both the L_α^C and H_{II}^C phases are observed, depending on the charge density and the softness of the constituting membranes. For lamellar complexes we find, in agreement with X-ray scattering data,[16] that the positional order is restricted to finite domains consisting of the order of 10 DNA molecules. Therefore, such complexes contain many grain boundaries and defects which may strongly influence the TE. Inverted hexagonal complexes appear much more ordered (again, consistent with X-ray experimental data);[17] however, their membranes do not form isolated tubular micelles around individual DNA rods but rather a space-filling continuous substructure. Upon decreasing the molar fraction of neutral (helper) lipids, the 2D hexagonal lattice of DNA rods melts, and a disordered structure with many structural defects appears. When all the neutral lipids (NLs) are removed, this disordered structure transforms into a novel phase not previously reported, where DNA rods and cylindrical micelles form a 2D square lattice analogous to the 3D cubic NaCl-type structure.

(17) Koltover, I.; Salditt, T.; Rädler, J. O.; Safinya, C. R. *Science* **1998**, *281*, 78–81.
(18) Lin, A. J.; Slack, N. L.; Ahmad, A.; George, C. X.; Samuel, C. E.; Safinya, C. R. *Biophys. J.* **2003**, *84*, 3307–3316.
(19) Ahmad, A.; Evans, H. M.; Ewert, K.; George, C. X.; Samuel, C. E.; Safinya, C. R. *J. Gene Med.* **2005**, *7*, 739–748.
(20) Farago, O.; Ewert, K.; Ahmad, A.; Evans, H. M.; Grønbech-Jensen, N.; Safinya, C. R. *Biophys. J.* **2008**, *95*, 836–846.
(21) Koynova, R.; Wang, L.; MacDonald, R. C. *Proc. Natl. Acad. Sci. U.S.A.* **2006**, *103*, 14373–14378.
(22) Ewert, K.; Evans, H. M.; Zidovska, A.; Bouxsein, N. F.; Ahmad, A.; Safinya, C. R. *J. Am. Chem. Soc.* **2006**, *128*, 3998–4006.
(23) Rajesh, M.; Sen, J.; Srujan, M.; Mukherjee, K.; Sreedhar, B.; Chaudhuri, A. *J. Am. Chem. Soc.* **2007**, *129*, 11408–11420.
(24) Bandyopadhyay, S.; Tarek, M.; Klein, M. L. *J. Phys. Chem. B* **1999**, *103*, 10075–10080.
(25) May, S.; Harries, D.; Ben-Shaul, A. *Biophys. J.* **2000**, *78*, 1681–1697.
(26) Lasic, D. D.; Strey, H.; Stuart, M. C. A.; Podgornik, R.; Frederik, P. M. D. *J. Am. Chem. Soc.* **1997**, *119*, 832–833.
(27) Safinya, C. R. *Curr. Opin. Struct. Biol.* **2001**, *11*, 440–448.
(28) Brannigan, G.; Lin, L.C.-L.; Brown, F. L. H. *Eur. Biophys. J.* **2006**, *35*, 104–124.
(29) Farago, O.; Grønbech-Jensen, N.; Pincus, P. *Phys. Rev. Lett.* **2006**, *96*, 018102.
(30) Farago, O.; Grønbech-Jensen, N. *Biophys. J.* **2007**, *92*, 3228–3240.

Modeling and Computational Details

The model studied in this work is based on the Noguchi−Takasu ISCG membrane model[31] that has been developed to mimic the hydrophobic effects of water through an energy penalty for low local hydrophobic solute density. This level of modeling is consistent with our previous work on complexes of DNA and charged lipid membranes,[20,29,30] and it provides for an appropriate balance between the discrete presence of elongated lipid molecules as the building blocks of flexible membranes and idealized molecular simplicity for practical simulations. Within the Noguchi−Takasu model, each lipid is represented by a rigid molecule consisting of three beads of diameter σ, one of which is hydrophilic and the other two of which are hydrophobic. In addition to short-range excluded volume interactions (that exist between every pair of beads), the hydrophobic beads interact via an attractive multibody potential which accounts for the hydrophobic, water-mediated, interactions. The Noguchi−Takasu model exhibit high self-assembly efficiency and readily forms large spherical micelles.[31] The equations of motion for the lipid beads are:

$$m_i\ddot{\bar{r}}_i + \alpha_i\dot{\bar{r}}_i = -\nabla_i U(\{\bar{r}_j\}) + \bar{n}_i(t) + \sum_k \bar{\Lambda}_{ik} \tag{1}$$

where $\bar{r}_i$ is the coordinate of the ith bead, m_i is its mass, α_i is its empirical friction coefficient, $U(\{\bar{r}_j\})$ is the interaction energy as a function of the coordinates of all particles. The thermal noise, denoted by $\bar{n}_i(t) = (n_{i,x}, n_{i,y}, n_{i,z})^T$ in the above equation, satisfies[32]

$$\langle \bar{n}_i(t) \rangle = \bar{0} \tag{2}$$

$$\langle n_{i,a}(t) n_{j,b}(s) \rangle = 2\alpha_i k_B T \delta(t-s)\delta_{ij}\delta_{ab} \tag{3}$$

where $a, b = x, y, z$, k_B is Boltzmann's constant, T is absolute temperature, and $\langle\ \rangle$ denotes statistical (thermal) average. Finally, $\bar{\Lambda}_{ik}$ represents the Lagrange multipliers that provide the constraints necessary for enforcing the rigid lipid geometry. An efficient algorithm for determining these for a linear molecular geometry can be found in ref 33. The DNA molecules are modeled as infinitely long parallel stiff rods in the z-direction. They are thus described as 2D objects whose motion in the (x,y)-plane is described by the same type of equation of motion as shown above for the lipid beads. However, unlike the lipids, the DNA rods have neither hydrophobic interactions nor do they involve any Lagrange multipliers.

The normalized (in k_BT units) interaction energy surface U is given by

$$U = U_{hyd} + U_{el} + U_{rep} \tag{4}$$

where U_{hyd} is the hydrophobic interaction potential outlined in ref 31. In adopting the Noguchi−Takasu representation of hydrophobicity, we have chosen the characteristic length unit $\sigma = 6.25$ Å. The normalized electrostatic energy U_{el} is

$$U_{el} = \frac{e^2}{4\pi\varepsilon_0\varepsilon_r\sigma k_B T}\sum_{i>j} u_{el}(r_{ij}/\sigma) \tag{5}$$

where ε_0 and $\varepsilon_r = 78$ are the vacuum and relative permittivity, respectively, e is the unit charge, and r_{ij}/σ is the normalized distance between the charged particles. The charge−charge interaction energy is given by:

$$u_{el}(r) = \begin{cases} q_i q_j / r & \text{for bead} - \text{bead interactions} \\ -2q_i\lambda_j \ln r & \text{for bead} - \text{DNA interactions} \\ -2\lambda_i\lambda_j L_z \ln r & \text{for DNA} - \text{DNA interactions} \end{cases} \tag{6}$$

Here, the fractional charge q_i (normalized to the unit charge e) represents the point charge of the i th bead, and λ_i is the normalized line charge density (to e/σ) for a DNA rod. All our simulations are conducted in a simulation box with dimension $(L_x, L_y, L_z)\sigma$, and all electrostatic contributions are evaluated with the complete resummation technique outlined in refs 34 and 35. Thus, the electrostatic DNA−DNA interaction is calculated for its contribution within the simulation box, which is the reason for the factor L_z in eq 6.

DNA rods are modeled as infinitely long and cylindrically symmetric with uniform charge density corresponding to −1.7 e/Å. Adopting the short-range repulsive bead−bead potential $U_{rep,bb}(r)$ from ref. 31, we model the bead−DNA short-range potential as $U_{rep,bD}(r) = U_{rep,bb}(r - 1.5\sigma)$. This corresponds to setting the DNA radius to $2\sigma = 12.5$ Å. We notice that, due to the large DNA line charge density, any DNA−DNA distance is always larger than the short-range hard-core repulsive contact. The CLs are modeled by associating the hydrophilic bead with a $+1e$ point charge. Charge neutrality of our simulations is ensured by choosing the number of CLs as well as the dimension L_z such that the total DNA charge is balanced by the total lipid charge in the simulation box. Thus, the simulations represent the isoelectric point of the phase diagram.

The objective of this work is to investigate how the above-mentioned rather simple model can produce the characteristics of the various observed self-assembled CL−DNA complexes. We emphasize that we are not expecting direct and detailed agreement with experiments, but instead are interested in a more generic investigation of hierarchical behavior that is a result of energetic and entropic competitions. To achieve this goal, we study the entire process of self-assembly from a random initial configuration of scattered lipids and DNA rods and follow the evolution of the complexes that form under different conditions. We investigate the evolution and structure of the complexes as a function of two different system parameters. One is the charge density of the cationic membrane, which can be controlled by changing the number of simulated NLs in the ensemble. The other is the stiffness of the membrane, which can be manipulated through a phenomenological energy penalty against angular variations between neighboring lipids. We choose the following form, where the (normalized) energy κ_s is the control parameter:

$$U_{bend} = 0.5\kappa_s \sum_{i>j} h(r_{ij}^{(cm)})(\bar{u}_i - \bar{u}_j)^2 \tag{7}$$

The sum in eq 7 runs over all pairs of lipids whose centers of mass are separated by a distance $r_{ij}^{(cm)}$ smaller than the cutoff length of the function h which determines the range of the hydrophobic interaction in the Noguchi−Takasu model. The unit vectors $\bar{u}_i$ and $\bar{u}_j$ represent the orientations of the lipids. This stiffening mechanism is similar to what was introduced in the later version of the Noguchi−Takasu model.[36] Like our previous studies of DNA−membrane complexes, the current model suffers from a significant geometrical constraint in the infinitely long and parallel DNA model molecules. This simplifying constraint provides for a computationally convenient choice of L_z, since we can decide only to simulate a thin slab of material in the direction along the DNA extension. Thus, most of our simulations are conducted with $L_z\sigma = 6.8\sigma = 42.5$ Å, which makes each simulated DNA rod represent a charge of $-25e$ within the simulation box. We simulate 32 DNA rods, which require 800 CLs to balance the charge. All simulations presented here have $L_x\sigma = L_y\sigma = 200\sigma = 125$ nm. Normalized masses and friction coefficients of the beads have been chosen to unity, while the DNA mass and friction coefficients (per L_z) have been chosen to 100 and 1000, respectively. These parameters provide for a natural separation between the mobilities of the DNA and the lipids

(31) Noguchi, H.; Takasu, M. *Phys. Rev. E* **2001**, *64*, 041913.
(32) Parisi, G. *Statistical Field Theory*; Addison-Wesley: New York, 1988.
(33) Tapia-McClung, H.; Grønbech-Jensen, N. *J. Polym. Sci. B: Polym. Phys.* **2005**, *43*, 911–916.
(34) Grønbech-Jensen, N. *Int. J. Mod. Phys. C* **1997**, *8*, 1287–1297.
(35) Grønbech-Jensen, N. *Comput. Phys. Commun.* **1999**, *119*, 115–121.
(36) Noguchi, H. *Phys. Rev. E* **2003**, *67*, 041901.

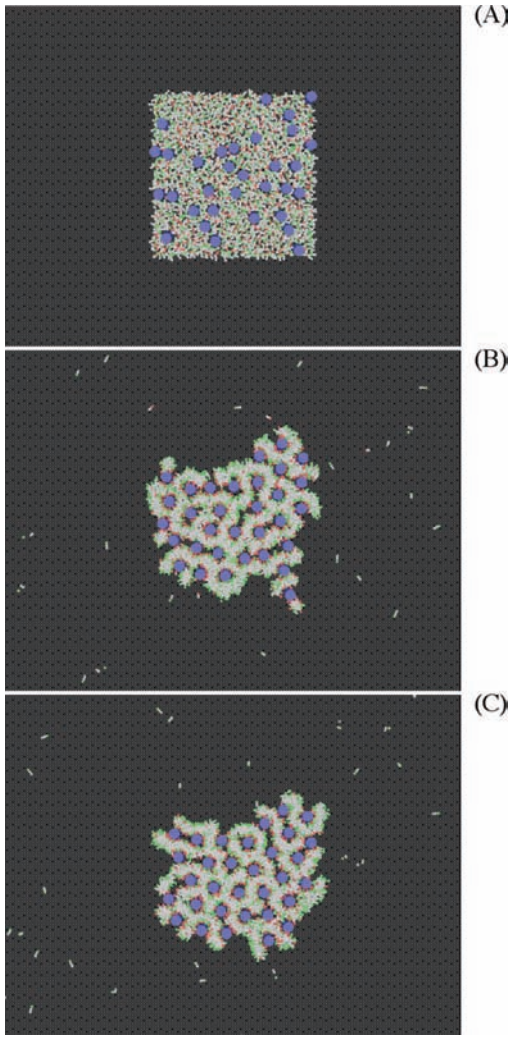

Figure 1. View along z-direction. Self-assembly evolution of a CL−DNA complex consisting of 800 CLs, 1600 NLs ($\phi_c = 1/3$), and 32 DNA rods. Stiffness parameter $\kappa_s = 0$. Color coding: gray - hydrophobic lipid beads, red - charged hydrophilic heads, green - neutral hydrophilic heads, and blue - DNA rods. The three configurations presented here show: (A) the densely packed random initial configuration, (B) a rapidly self-assembled structure, after 10^6 MD time steps, consisting of bilayer membranes whose cationic charge is in strong association with the DNA rods, and (C) hexagonal CL−DNA complex formed after a long self-assembly process of 21×10^6 MD time steps.

throughout the simulations, without influencing the final equilibrium states. Simulations are initiated such that all DNA rods and lipids are randomly positioned (and randomly oriented for lipids) within a densely packed region with no particle overlap allowed. The simulations then progress guided only by the energetics and the thermal noise using a Verlet integrator with adaptive time step control such that no particle moves more than about 0.05σ per numerical time step.

Results

The progression of a typical simulation run can be viewed in Figure 1, where we show an (x, y) plot of the system (a view of the system from the z-direction) at different times. In this example the stiffness parameter $\kappa_s = 0$, and the fraction of CLs is $\phi_c = 1/3$, which corresponds to 1600 NLs (twice as many than the number of CLs). The color coding is: hydrophobic lipid beads (gray), charged hydrophilic heads (red), neutral hydrophilic heads (green), and DNA rods (blue). We here observe

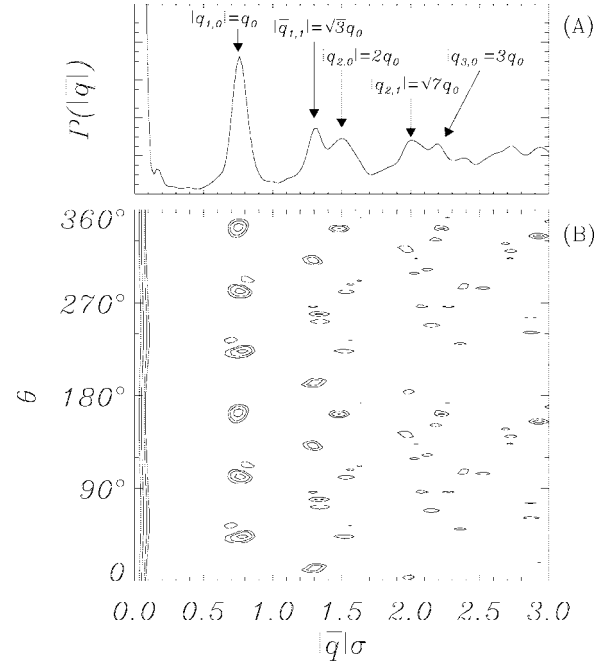

Figure 2. Simulated scattering density of the structure shown in Figure 1C. Scattering density $P(\bar{q}) = \langle|\mathscr{F}|^2\rangle(\bar{q})|\bar{q}|\exp(-i\theta))$ is acquired from eq 8, averaged over 20,000 consecutive MD time steps. (A) Angle averaged density $P(|\bar{q}|) \equiv (1/2\pi)\int_0^{2\pi} P(\bar{q})d\theta$. (B) Contour plot of $P(\bar{q})$. Bragg peaks of the hexagonal structure are indicated in (A).

the confined initial random configuration in Figure 1A. Very quickly, the system arranges itself in order to provide electrostatic self-screening and in order to minimize hydrophobic exposure to the solvent. These two objectives result in rapid formation of a disordered complex structure consisting of bilayer membranes whose cationic charge is strongly associated with the DNA rods (see Figure 1B). Over longer time scales (Figure 1C) the hydrophobic effect provides for a larger-scale self-assembly into a structure in which the DNA positions are ordered relative to each other; in this case a hexagonal structure where the DNA rods are separated as distance d_{DNA} from each other, and the spacing between them is almost entirely occupied with hydrophobic lipid material.

The hexagonal structure shown in Figure 1C is visually obvious, so it is of interest to investigate how this structure will appear in a simulated diffraction plot. Figure 2 shows the Fourier transformations of the DNA positions $\bar{r}_j$:

$$\mathscr{F}(\bar{q}) \propto \sum_{j=1}^{N_{DNA}} e^{i\bar{r}_j\bar{q}} \tag{8}$$

averaged over a time interval of 20,000 MD time steps. This time interval is short compared to any significant transport of DNA, so the choice of this time average has been made to smooth any temporary jitter in the DNA configuration while making sure that the resulting averaged Fourier transform is representative of overall structure seen in the figures. Figure 2B displays the scattering density $P = |\mathscr{F}|^2$ as a function of the reciprocal vector $\bar{q} = |\bar{q}|\exp(-i\theta)$, and Figure 2A shows the average of the density over all angles θ. The Bragg peaks in Figure 2A can be indexed with a hexagonal lattice of $d_{DNA} \approx 10\sigma$: $q_{1,0} = q_0 = 4\pi/(\sqrt{3}d_{DNA})$, $q_{1,1} = \sqrt{3}q_0$, $q_{2,0} = 2q_0$, $q_{2,1} = \sqrt{7}q_0$, $q_{3,0} = 3q_0$. The scattering signatures for the inverted hexagonal phase can be also traced in the distinct contour peaks of Figure 2B, which can be related to the peaks in the 1D

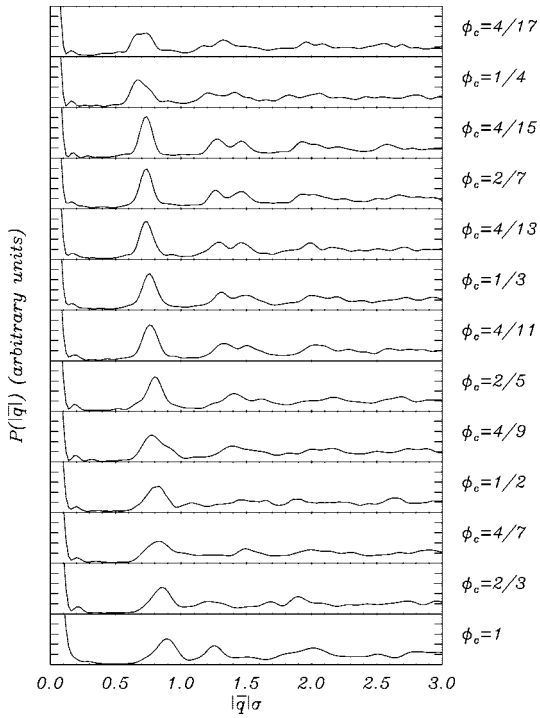

Figure 3. Simulated angle-average scattering density $P(|\bar{q}|)$ calculated from an average of 20,000 consecutive MD time steps for different charge densities ϕ_c and $\kappa_s = 0$. Each scattering plot is obtained after a simulation run of $20-80 \times 10^6$ MD time steps.

averages shown in Figure 2A. For $|\bar{q}| = q_0$, the scattered intensity is peaked at six angles that are separated by 60° intervals from one another, indicating the directions of the reciprocal hexagonal lattice. We notice that the observed peak at $q_{1,0} \approx 0.725\sigma^{-1}$ corresponds to $d_{DNA} \approx \delta_m + D \approx 10\sigma = 62.5$ Å, where $\delta_m \approx 2 \times 3\sigma = 6\sigma$ is the width of the bilayer membrane (roughly twice the length of the lipids) and $D = 4\sigma$ is the diameter of the DNA rod.

We can now show a collection of simulation data by displaying the angle-averaged scattering intensity, $P(|\bar{q}|)$, for a variety of lipid charge densities. This is done in Figure 3, where we show results from the fully charged case $\phi_c = 1$ down to the relatively dilute regime ($\phi_c = 4/17$). We find the characteristic signatures of hexagonal DNA ordering in the charge density regime of $4/15 \leq \phi_c \leq 2/5$; i.e., the inverted hexagonal phase seems to spontaneously self-assemble for moderate charge densities. We also observe how the characteristic density peaks appear to move to slightly smaller values of $|\bar{q}|$ (i.e., larger d_{DNA}) as the charge density of the lipids decreases, i.e., as the number of NLs is increased. This is consistent with the simple hydrophobic space-filling purpose that the NLs serve in forming the inverted hexagonal phase. The swelling of the hexagonal complex upon addition of NLs is, however, limited since, within the inverted hexagonal phase, the preferred inter-DNA spacing must satisfy $d_{DNA} \approx \delta_m + D$. The structures for lipid charge densities outside the range of the hexagonal structure can be explained along similar lines: In the dilute limit (small ϕ_c), the space filling by an increasingly larger amount of NLs leads to larger fluctuations in inter-DNA distances. These variations eventually overwhelm the coherency of the long-range order observed in Figure 1C, and the result can be seen in Figure 4 for $\phi_c = 4/17$. In this representative configuration the hexagonal order persists only locally. One can also observe that the system exhibits a large number of structural defects, some of which

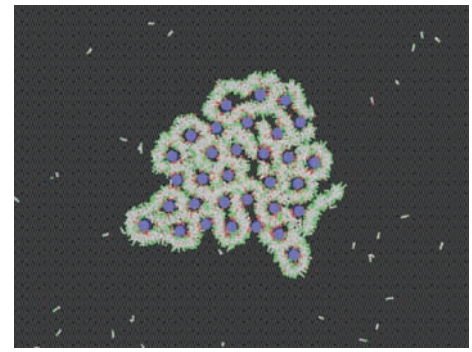

Figure 4. Representative structure of the CL−DNA complex that gives the scattering intensity shown in Figure 3 for $\phi_c = 4/17$. This structure is obtained after approximately 31×10^6 simulated MD time steps.

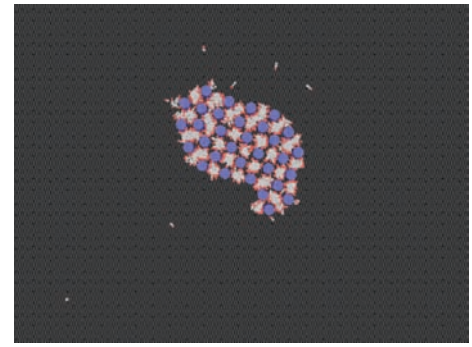

Figure 5. Fully charged complex ($\phi_c = 1$) with a square lattice arrangement of DNA rods and cylindrical micelles. This structure is obtained after approximately 83×10^6 MD time steps.

can be related to the boundaries between microphase-separated regions of (i) closely packed hexagonal structure and (ii) excess NLs that form neutral bilayer membranes. It is interesting to note that a similar phenomenon, namely local phase separation of excess NLs, has been recently observed in studies of complexes of multivalent CLs and DNA.[20] In the highly charged lipid limit (large ϕ_c) the system is depleted of neutral hydrophobic filler material. The high-charge cationic density causes large mechanical tensile stresses which, in turn, lead to Rayleigh-like instability[37] and membrane rupture (see refs 29 and 30). As a result of the fragmentation of the membrane, the complex may collapse into a high charge density ordered structure with quadratic order of DNA, where DNA and tubular micelle-like lipid arrangements form the structure viewed in Figure 5. To the best of our knowledge, this novel phase of CL−DNA complexes has not been previously reported. The square lattice arrangement shown in Figure 5 achieves the two primary objectives of the self-assemble process, namely to avoid hydrophobic exposure to the solvent and to optimize the electrostatic energy by minimizing the charge separation between the DNA rods and the cationic headgroups of the lipids. The addition of NLs drives the system from the square lattice into the hexagonal structure in which these objectives are also realized, but at a lower bending energy cost.

As noted in ref 36, the original lipid model that we have adopted above produces a very soft membrane, i.e., a membrane with a very low bending modulus. In order to study the self-assembly of complex structures involving stiffer membranes,

(37) Nguyen, T. T.; Gopal, A.; Lee, K. Y. C.; Witten, T. A. *Phys. Rev. E* **2005**, *72*, 051930.

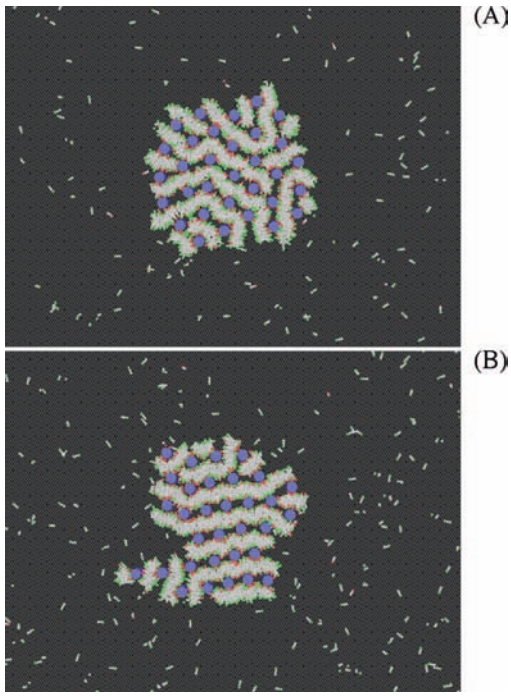

Figure 6. (A) Complex structure formed after 16×10^6 MD time steps at charged density $\phi_c = 4/13$ with stiffness parameter $\kappa_s = 2.5$. (B) Complex structure formed after 16×10^6 MD time steps at charged density $\phi_c = 4/13$ with stiffness parameter $\kappa_s = 5$. In (B) the DNA rods form a face-centered rectangular lattice, while the lipids are arranged in a lamellar structure of nearly flat bilayers.

we now include the phenomenological stiffness mechanism depicted by eq 7, which provides an energetic penalty for misaligned neighboring lipids. This penalty enhances the membrane stiffness as κ_s is increased from zero. We have conducted several series of simulations for $\kappa_s > 0$ similar to the ones described above for $\kappa_s = 0$. These simulations indicate, in agreement with experimental results[17] that, as the stiffness of the membrane is increased, the complex undergoes a phase transition from inverted hexagonal to lamellar structure. This transition is illustrated in Figure 6 for $\phi_c = 4/13$, with (A): $\kappa_s = 2.5$, an intermediate structure incorporating features of both the inverted hexagonal and lamellar phases, and (B): $\kappa_s = 5$, what appears to be lamellar membrane ordering. In terms of the DNA ordering, the lamellar structure shown in Figure 6B has characteristics very similar to those of the hexagonal structure discussed above. Specifically, the DNA rods form a centered rectangular structure where the aspect ratio between the lattice basis vectors is quite close to unity (which is the aspect ratio between the basis vectors of the hexagonal lattice). The major difference between the hexagonal and the lamellar structures is the membrane material, which in the stiffer model forces the straight membrane segments to open layered pores in which the DNA rods can exist. These differences in the space-filling distribution of the lipids throughout the complex are clearly seen in a comparison of Figures 1C and 6B. One should pay special attention to the distributions of the CLs in the two phases. The rigidity of the membranes in the lamellar phase prevents the CLs from being evenly distributed around the DNA rods. These observation are consistent with previous theoretical and experimental studies[25−27] which demonstrated that (i) the local neutralization of the DNA charges by the CLs makes the inverted hexagonal phase more favored by electrostatic interaction and (ii) this energy gain is offset by the curvature elastic energy that drives the system into the lamellar phase.

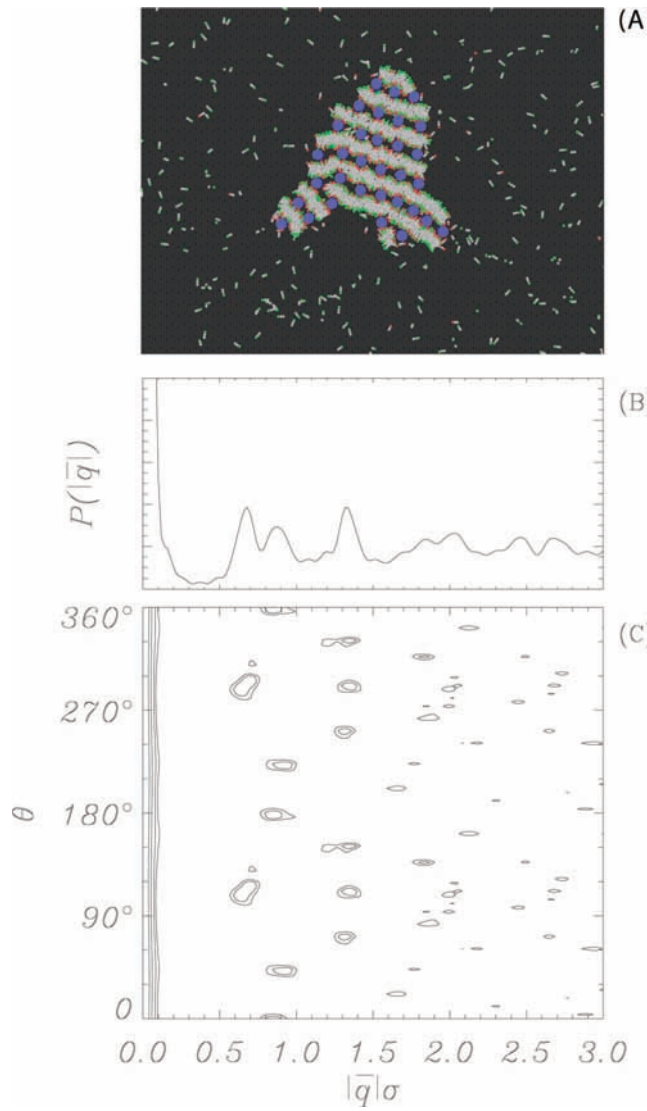

Figure 7. (A) Complex structure formed after 25×10^6 MD time steps at charged density $\phi_c = 1/3$ with stiffness parameter $\kappa_s = 10$. DNA rods form a face-centered rectangular lattice, while the lipids are arranged in a lamellar structure of nearly flat bilayers. (B) Scattering intensity $P(|\bar{q}|)$ averaged over 20,000 consecutive MD time steps and all angles of $\bar{q}$. (C) Contour plot of scattering intensity $P(\bar{q})(\bar{q} = |\bar{q}| \exp(-i\theta))$ averaged over 20,000 consecutive MD time steps. Scattering intensity peaks are discussed in the text.

Figure 7A shows the complex formed at charge density $\phi_c = 1/3$ for $\kappa_s = 10$, along with the corresponding simulated scattering data (B and C of Figure 7). Here, we clearly observe the strong lamellar orientation and the registry between the DNA positions in different membrane layers. More precisely, the DNA arrangement can be identified as a centered-rectangular lattice with one basis vector ($\bar{a}_1$) connecting nearest-neighbor rods along the same layer, and the other ($\bar{a}_2$) joining next-nearest neighbors that lie within adjacent layers. The aspect ratio between the two basis vectors $r = |\bar{a}_2|/|\bar{a}_1| \simeq 4/3$. The first three diffraction peaks in Figure 7B can be explained as follows: The first peak is centered around $q_0 = 4\pi/d_{DNA}$ and is associated with the two opposite Bragg angles (see Figure 7C) of the (1,0) crystallographic directions. The second peak which can be related to the (0,1) direction is observed at four different angles and at wave vector $|\bar{q}| = rq_0$. The third peak is due to scattering

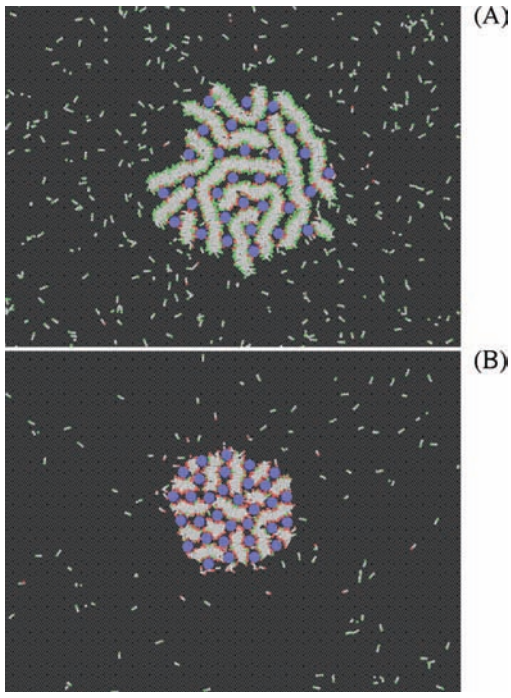

Figure 8. Complex structures for stiffness parameter $\kappa_s = 10$ at (A) low lipid charge density ($\phi_c = 4/17$) after 15×10^6 MD time steps and (B) high charge density ($\phi_c = 4/7$) after 26×10^6 MD time steps.

from six Bragg angles, including (i) the two angles of the (2,0) crystallographic directions (which are identical to the (1,0) directions) at $|\bar{q}| = 2q_0$, and (ii) four angles of the (1,1) crystallographic directions at $|\bar{q}| = (2 + r^2)^{1/2}q_0 \simeq 1.95q_0$. In analogy with what is shown in Figure 2, we have conducted a set of simulations for systems with $\kappa_s = 10$ and different charge densities (not shown here). The results indicate that the lamellar structure is formed in the regime of moderate charge densities ($\phi_c \approx 1/3$). As was the case with the hexagonal structure observed for $\kappa_s = 0$, the formation of the lamellar structure is also inhibited by both small and large charge densities. In the diluted limit (see Figure 8A), large DNA distances along the lamellar direction result in an erosion of the definition and orientation of the lamellar ordering. The limit of high ϕ_c (Figure 8B) brings the system back to the regime where the strong tensile stress in the membrane gives rise to rupture and resulting destruction of the long-range order of the lamellas.

One can envision further increasing the stiffness of the membrane through the parameter κ_s in order to compensate for the membrane bending, but Figures 7 and 8 allude to an emerging problem with this strategy within the Noguchi−Takasu ISCG model. As the stiffness κ_s of the model membrane is increased, we notice an unrealistically increased dissolution of the lipids, which arises from the entropic difficulty of membrane assembly when the energetic penalty for angular disorder becomes too large. It simply becomes too improbable for the lipids to collectively aggregate with the right relative angles. Thus, while an increase in this type of stiffness mechanism does produce a stiff membrane, it will eventually also produce entropic dissolution of the membrane. We have found that this parametrization of the model system does not support stable membranes for κ_s much larger than what is shown in this work.

Conclusion

In summary, we have provided a comprehensive set of simulations that elucidates several features of experimentally observed self-assembled structures in solutions of DNA and mixtures of neutral and cationic lipids. These mesoscale simulations have been based on a simple coarse-grained model of idealized model lipids and DNA rods. The fact that this simplified model can produce self-assembly of several characteristic configurations illustrates that the underlying mechanisms for the complex structures lie in the inherent competition between hydrophobicity, electrostatics, entropy, and molecular geometry. Our studies have provided a partial glimpse of a phase diagram in which lamellar and hexagonally packed DNA can be found for intermediate charged lipid densities, whereas large amounts of neutral lipids seem to dilute the spatial order, and too small amounts of neutral lipids results in membrane rupture. Soft membrane material results in a square DNA packing for very high lipid charge density. We emphasize that, while the current coarse-grained model system produces *qualitative* agreement with the experimentally observed trends in the phase diagram of the system, it cannot provide detailed *quantitative* results for direct comparisons with complexes of specific lipids compositions under different buffer conditions. To probe the detailed behavior of specific lipoplexes (see, e.g., experiments reported in refs 21 and 23) one must use atomistic[24] or less coarse-grained[38] models employing force fields that represent the specific interactions between the biomolecular entities. Unfortunately, the computational cost of these atomistic simulations is enormous which makes simulations of large complexes using these tools prohibitively expensive. In contrast, the computational simplicity and efficiency of our coarse-grained model and the intuitively correct qualitative results arising from our simulations make our modeling approach suitable and appealing for large length- and time-scale simulations of CL−DNA complexes, as well as for other complex supramolecular structures.

Acknowledgment. We thank Cyrus Safinya for many enlightening and invaluable discussions during the completion of this work. This work was supported by the Israel Science Foundation (Grant Number 946/08).

JA807278P

(38) Khalid, S.; Bond, B. J.; Holyoake, J.; Hawtin, R. W.; Sanson, M. S. P. *J. R. Soc. Interface* **2008**, *5*, S241–S250.